Effect of atomic recoil on the absorption spectrum of driven V-type atoms

Hong Y. Ling and Anthony Williams
Department of Chemistry and Physics, Rowan University, Glassboro, New Jersey 08080
(Received 29 April 1999)

A numerical method is developed for a V system driven by two counterpropagating laser fields in a momentum regime where a full quantum-mechanical treatment of the atomic variables is necessary. This method is based on a transformation by which integral equations, reduced from steady-state optical-Bloch-type equations involving the atomic center-of-mass momentum, can be transformed into inhomogeneous tridiagonal vector recurrence equations. The effect of the atomic recoil on the momentum distribution in the absence of the probe field, and, in particular, the absorption spectrum in a copropagating spectrum configuration is analyzed and discussed. Special attention is given to the Rayleigh resonance of subnatural linewidth.
[S1050-2947(99)10112-4]

PACS number(s): 32.80.Pj, 32.70.−n, 42.50.−p, 42.65.−k

I. INTRODUCTION

An atom can experience a recoil during the absorption and emission of radiation as a consequence of the momentum conservation. This atomic recoil plays an essential role in the laser cooling of atoms [1]. Laser cooling and trapping of atoms eventually led to the recent spectacular display of Bose-Einstein condensation of gaseous atoms [2–5]. Cold atoms enjoy much reduced Doppler and transit broadenings, and, therefore, are ideal for nonlinear spectroscopy. The Lamb-Dick narrowing was observed by Westbrook *et al.* [6] in a fluorescence spectroscopic experiment involving cold Na atoms in three-dimensional (3D) standing waves. Dispersionlike resonances of subnatural linewidth were reported, independently, by Grison *et al.* [7] and Tabosa *et al.* [8], in the absorption spectrum of cold cesium atoms in 3D magneto-optical traps. Effects similar to those in Refs. [6–8] were also demonstrated by Verkerk *et al.* [9] and analyzed by Courtois and Grynberg [10] in 1D laser cooling of cesium atoms under different polarization configurations. Recoil-induced resonances, first predicted by Guo and co-workers [11,12], were later observed experimentally by Courtois *et al.* [13]. More recently, a collective-atomic-recoil laser (CARL) was proposed by Bonifacio and co-workers [14–16] in an effort to convert atomic kinetic energies into coherent radiation. This has sparked a series of activities, both experimental [17,18] and theoretical [19–21], surrounding CARL.

In this paper, we study the effect of atomic recoil on the momentum distribution and, especially, the absorption spectrum of cold V atoms driven by nearly resonant counterpropagating pump fields. The absorption spectrum is calculated in a copropagating spectrum configuration in which the probe induces the same atomic transition as the copropagating pump field. The study is intended to be fully quantum mechanical in the sense that quantization is performed on both the internal and external degrees of atomic freedom. Such a treatment leads to the generalized optical Bloch (GOB) equation for the atomic variables involving the center-of-mass atomic momentum. To justify this approach, we follow Ref. [22] and limit our study to atoms that have relatively narrow atomic lines and are precooled to within several Doppler cooling limits. Compared to many multilevel systems [6–9,11,12], our system does not allow a photon of one direction to be transferred, by stimulated processes, into a photon of opposite direction, a phenomenon known as coherent photon redistribution. Coherent photon redistribution is indeed forbidden in *W* systems driven by counterpropagating σ_+-and σ_--polarized fields [23,24] in a copropagating spectrum configuration. However, in these studies, the pump fields are assumed to be far off resonance, and the calculation is not fully quantum mechanical.

The ''nearly resonant'' requirement makes it difficult to apply adiabatic or secular approximations to simplify GOB-type equations. In addition, we also leave the arbitrary laser intensity open, so that the results from the dressed-state theory [25–27] may be tested for very cold atoms. For these reasons, it is very difficult to carry out this study in an analytical manner. The numerical simulation at long time can be problematic [28]. In general, as the interaction time increases, on the one hand, one has to increase the sampling rate so that the narrow peaks in the momentum distribution caused by laser cooling are not smeared; on the other hand, one must increase the momentum domain to accommodate the momentum diffusion by spontaneous emission. This will inevitably lead to a large number of coupled equations (in the momentum space) at long time. If one simply takes a numerical integration of GOB equations to find the steady-state solution, it will be very time consuming. In this paper, we follow Refs. [11,12,29,30] and approximate the transit process with a decay rate γ_t (much smaller than any relevant rates) and a momentum distribution $W(p)$, so that a steady-state solution can always be reached in about γ_t^{-1} time. Under such a circumstance, one can, in principle, obtain the steady-state solution by solving linear matrix equations. However since the dimension of matrices at long time, as just noted, can be large, one may encounter problems inherent from sparse matrices of large dimension [31]. One can also follow Refs. [29], [32] to reduce the coupled steady-state GOB equations into an integral equation involving a single unknown function, and to solve it by an iterative method based on the concept of perturbation. However, this approach has a low rate of convergence, especially at long time and with relatively large pump laser intensities.

In this paper, we develop an alternative method to solve

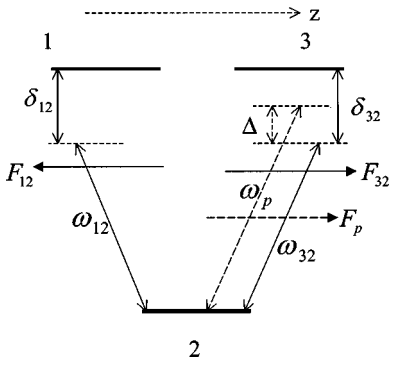

FIG. 1. A schematic diagram of three-level V-type atoms driven by two counterpropagating pump laser fields (solid arrows) and probed by a weak field (dashed arrows).

steady-state GOB-type equations. This method can be divided into two stages. In the first stage, we basically follow Refs. [29], [32] and derive a single integral equation from the coupled GOB equations. In the second stage, we transform the integral equation into an inhomogeneous tridiagnal vector recurrence equation, and solve it by the method of matrix continued fraction [33,34]. The method of (matrix) continued fraction, although popular among the semiclassical laser-cooling studies [35,36], has, to our knowledge, never been generalized to the spectroscopic calculation of atoms in a full quantum-mechanical description. The virtue of this method is that, no matter how large the momentum space, the dimension of all the matrices involved is limited to the number of divisions within $2\hbar k$, a subspace typically much smaller than the relevant momentum space. This paper is organized as follows. In Sec. II, we introduce our model and present the GOB equations along with the absorption spectrum formula. Sections III and IV are devoted to the reduction of steady-state GOB-type coupled equations into single integral equations that are essential to the calculation of the atomic momentum distribution and absorption spectrum. The numerical method will be outlined in Sec. V. Section VI presents and discusses the numerical results, with an emphasis placed on recoil-related phenomena. A brief summary is provided in Sec. VII.

II. THEORETICAL MODEL AND EQUATIONS OF MOTION

Figure 1 shows a schematic diagram of a degenerate driven V system. The dipole allowed transitions are driven, independently, by pump laser fields of frequencies ω_{32} and ω_{12}, wave vectors k and $-k$, and amplitudes F_{32} and F_{12}. In addition, a weak probe field of frequency ω_p, wave vector k, and amplitude F_p is applied between levels 3 and 2. F_{12}, F_{32}, and F_p are slowly-varying amplitudes of space and time defined in the expansion for the total field,

$$\hat{\mathbf{F}}(\hat{z},t)=\tfrac{1}{2}(\vec{e}_{32}F_{32}e^{-i\omega_{32}t+ik\hat{z}}+\vec{e}_{12}F_{12}e^{-i\omega_{12}t-ik\hat{z}}+\vec{e}_{32}F_pe^{-i\omega_pt+ik\hat{z}})+\text{H.c.}, \tag{1}$$

where the fields are polarized in such a way that $\mu_{32}=\langle 3|\hat{\boldsymbol{\mu}}\cdot\vec{e}_{32}|2\rangle$ and $\mu_{12}=\langle 1|\hat{\boldsymbol{\mu}}\cdot\vec{e}_{12}|2\rangle$ (along with their complex conjugates) are the only surviving matrix elements of a dipole operator $\hat{\mu}$. We choose to work in a space spanned by $|i,p\rangle$, where i is the index to the internal atomic energy level, and p is the momentum eigenvalue of the atomic center-of-mass momentum operator. In this space, the atomic Hamiltonian

$$\hat{H}_A=\sum_i\int dp\left(\hbar\Omega_{i2}+\frac{p^2}{2M}\right)|i,p\rangle\langle p,i|, \tag{2}$$

is diagonalized, where $\hbar\Omega_{i2}$ is the energy of level i relative to the ground energy, while the interaction Hamiltonian, $\hat{H}_{L-A}=-\hat{\boldsymbol{\mu}}\cdot\hat{F}$, under the rotational-wave approximation, is reduced to

$$\hat{H}_{L\text{-}A}=-\int dp(\hbar E_{12}e^{-i\omega_{12}t}|1,p-\hbar k\rangle\langle p,2|+\text{H.c.}) \tag{3}$$

$$-\int dp(\hbar E_{32}e^{-i\omega_{32}t}|3,p+\hbar k\rangle\langle p,2|+\text{H.c.})$$

$$-\int dp(\hbar E_pe^{-i\omega_pt}|3,p+\hbar k\rangle\langle p,2|+\text{H.c.}), \tag{4}$$

where $E_{12}=\mu_{12}F_{12}/2\hbar$, $E_{32}=\mu_{32}F_{32}/2\hbar$, and $E_p=\mu_{32}F_p/2\hbar$ are the Rabi frequencies of the corresponding fields. The time evolution of the atomic density-matrix operator, ρ', in Schrödinger's picture, is governed by

$$\frac{d\rho'}{dt}=-\frac{i}{\hbar}[\hat{H}_A+\hat{H}_{L\text{-}A},\rho']+\left(\frac{s\rho'}{dt}\right)_{inc}, \tag{5}$$

where $(d\rho'/dt)_{inc}$ is the short-hand notation for random fluctuation and transit interaction. For simplicity, the transit process is simulated with a decay rate γ_t, sufficiently small so that γ_t^{-1} can be regarded as the interaction time resulting, for example, from atoms entering and leaving the interaction region [11,12,29], and an external pumping rate to the ground level, $\gamma_tW(p)$, where $W(p)$ is the normalized atomic momentum distribution in the absence of any coherent fields. As usual, the effect of random fluctuation is described by the population decay rate from level e to 2, Γ_{e2}, the lifetime of the level e, $\Gamma_e^{-1}=(\gamma_t+\Gamma_{e2})^{-1}$, and the relevant dephasing rates $\gamma_{e2}=\gamma_t+\Gamma_{e2}/2$ and $\gamma_{31}=\gamma_t+(\Gamma_{12}+\Gamma_{32})/2$, where $e=1$ or 3. Following the concept of momentum family [37,29], we introduce a set of slowly varying density-matrix elements:

$$\begin{aligned}
\rho_{11}(p,t)&=\rho'_{11}(p-\hbar k,p-\hbar k),\\
\rho_{22}(p,t)&=\rho'_{22}(p,p),\\
\rho_{33}(p,t)&=\rho'_{33}(p+\hbar k,p+\hbar k),\\
\rho_{21}(p,t)&=\rho'_{21}(p,p-\hbar k)e^{-i\omega_{12}t},\\
\rho_{23}(p,t)&=\rho'_{23}(p,p+\hbar k)e^{-i\omega_{32}t},\\
\rho_{13}(p,t)&=\rho'_{13}(p-\hbar k,p+\hbar k)e^{i(\omega_{12}-\omega_{32})t},\\
\rho_{ji}(p,t)&=\rho^*_{ij}(p,t)\quad\text{if } i\neq j,
\end{aligned} \tag{6}$$

where $\rho'_{ij}(p,p')=\langle p,i|\hat{\rho}'|j,p'\rangle$. Equations (2)–(5) along with the consideration of transit and random interactions result in the following GOB equations:

$$\frac{d}{dt}\rho_{11}(p,t)=-\Gamma_1\rho_{11}(p,t)+i[E_{12}\rho_{21}(p,t)-\text{c.c.}], \tag{7a}$$

$$\frac{d}{dt}\rho_{33}(p,t)=-\Gamma_3\rho_{33}(p,t)+i[E_{32}\rho_{23}(p,t)-\text{c.c.}]+i[E_p e^{-i\Delta t}\rho_{23}(p,t)-\text{c.c.}], \tag{7b}$$

$$\frac{d}{dt}\rho_{12}(p,t)=-\nu_{12}(p)\rho_{12}(p,t)+iE_{12}[\rho_{22}(p,t)-\rho_{11}(p,t)] \tag{7c}$$

$$-iE_{32}\rho_{13}(p,t)-iE_p e^{-i\Delta t}\rho_{13}(p,t), \tag{7d}$$

$$\frac{d}{dt}\rho_{32}(p,t)=-\nu_{32}(p)\rho_{32}(p,t)+iE_{32}[\rho_{22}(p,t)-\rho_{33}(p,t)] \tag{7e}$$

$$-iE_{12}\rho_{31}(p,t)+iE_p e^{-i\Delta t}[\rho_{22}(p,t)-\rho_{33}(p,t)], \tag{7f}$$

$$\frac{d}{dt}\rho_{31}(p,t)=-\nu_{31}(p)\rho_{31}(p,t)+i[E_{32}\rho_{21}(p,t)-E_{12}^*\rho_{32}(p,t)]+iE_p e^{-i\Delta t}\rho_{21}(p,t), \tag{7g}$$

$$\begin{aligned}\frac{d}{dt}\rho_{22}(p,t)=&\Gamma_{12}\int_{-\hbar k}^{+\hbar k}dqN(q)\rho_{11}(p+\hbar k+q,t)\\&+\Gamma_{32}\int_{-\hbar k}^{+\hbar k}dqN(q)\rho_{33}(p-\hbar k+q,t)\\&-\gamma_t\rho_{22}(p,t)+\gamma_t W(p)\\&-i[E_{12}\rho_{21}(p,t)-\text{c.c.}]\\&-i[E_{32}\rho_{23}(p,t)-\text{c.c.}]\\&-i[E_p e^{-i\Delta t}\rho_{23}(p,t)-\text{c.c.}].\end{aligned} \tag{7h}$$

Here, in addition to $\Delta=\omega_p-\omega_{32}$, we have introduced

$$\nu_{12}(p)=\gamma_{12}-i\delta'_{12}(p),\delta'_{12}(p)=\delta_{12}+\frac{k}{M}p, \tag{8a}$$

$$\nu_{32}(p)=\gamma_{32}-i\delta'_{32}(p),\delta'_{32}(p)=\delta_{32}-\frac{k}{M}p, \tag{8b}$$

$$\nu_{31}(p)=\gamma_{31}-i\delta'_{31}(p),\delta'_{31}(p)=\delta'_{32}(p)-\delta'_{12}(p), \tag{8c}$$

$$\nu_{ji}(p)=\nu_{ij}(p)^* \quad \text{if } i\neq j, \tag{8d}$$

where $\delta'_{12}(p)$, $\delta'_{32}(p)$, and $\delta'_{31}(p)$ are the Doppler-shifted laser detunings, and $\delta_{12}=\omega_{12}-\Omega_{12}-\omega_r$ and $\delta_{32}=\omega_{32}-\Omega_{32}-\omega_r$ are the laser detunings with respect to the recoil frequency shift $\omega_r=\hbar k^2/2M$. The atomic momentum redistribution by spontaneous emission is summarized in the integrations in Eq. (7h). Due to the randomness in the spontaneous emission, an excited atom of momentum $p+q$ with $q\leqslant|\hbar k|$ has the $N(q)$ probability of becoming a ground atom of momentum p, where

$$N(q)=\frac{3}{8\hbar k}\left[1+\left(\frac{q}{\hbar k}\right)^2\right], \tag{9}$$

assuming the emitted photons to be σ_+ or σ_- polarized [22].

To calculate the absorption spectrum of the probe field, we follow the perturbative approach [38] by expanding

$$\rho_{ij}(p,t)=\rho_{ij}^{(0)}(p)-i[E_p\rho_{ij}^{(1)}(p,\Delta)e^{-i\Delta t}-E_p^*\rho_{ij}^{(1)}(p,-\Delta)e^{i\Delta t}], \tag{10}$$

correct to the first order in the amplitude of the probe field, where $\rho_{ij}^{(0)}(p)$ is the steady-state solution without the probe field, and $\rho_{ij}^{(1)}(p,\Delta)[\rho_{ij}^{(1)}(p,-\Delta)=\rho_{ji}^{(1)*}(p,\Delta)]$ is the probe induced modulation at the frequency Δ and in the unit of $-iE_p$ (and hence is independent of E_p). The equations for $\rho_{ij}^{(0)}(p)$ and $\rho_{ij}^{(1)}(p,\Delta)$ can be derived from Eq. (8) and are left in Appendix A as references. The absorption spectrum in the context of this study shall be directly related to the macroscopic polarization at position z, given by $P_{32}(z,t)=\mu_{23}\rho'_{32}(z,t)+\text{c.c.}$, where $\rho'_{32}(z,t)$ is the density-matrix element in the position space, and can be obtained by the transformation [11]

$$\rho'_{32}(z,t)=\frac{1}{2\pi\hbar}\int\int dp\,dp'\exp\left[i\frac{(p'-p)z}{\hbar}\right]\rho'_{32}(p',p). \tag{11}$$

In this problem, because of the absence of the coherent photon redistribution, and the assumption that the loaded atoms are distributed uniformly over the space, $\rho'_{32}(p',p)$ is nonzero only if $p'=p+\hbar k$. This fact together with the definitions for the slowly varying density-matrix elements, allows us to arrive at

$$\rho'_{32}(p',p)=\rho_{32}(p)e^{-i\omega_{32}t}\delta(p'-p-\hbar k). \tag{12}$$

A polarization component $\rho'_{32}(z,\Delta,t)$, given by

$$\rho'_{32}(z,\Delta,t)=-iE_p\frac{1}{2\pi\hbar}\left[\int\rho_{32}^{(1)}(p,\Delta)dp\right]e^{-i\omega_p t-ikz},$$

is seen to oscillate at the frequency and travel along the direction of the probe field, when Eq. (12) is inserted into Eq. (11) and $\rho_{32}(p)$ is replaced with its perturbative expansion [Eq. (10)]. In analogy with the absorption coefficient introduced in the semiclassical theory, we define the absorption spectrum (at an arbitrary unit) as

$$\alpha(\Delta)=\text{Re}\left[\int\rho_{32}^{(1)}(p,\Delta)dp\right]. \tag{13}$$

III. INTEGRAL EQUATION FOR $\rho_{22}^{(0)}(P)$

In this section, we seek to derive, from Eqs. (A1), an integral equation for $\rho_{22}^{(0)}(p)$ along with the relations that can facilitate its numerical implementation outlined in Sec. V. We begin by substituting $\rho_{12}^{(0)}(p)[\rho_{21}^{(0)}(p)]$ and $\rho_{32}^{(0)}(p)[\rho_{23}^{(0)}$

$\times(p)]$, obtained from Eqs. (A1c) and (A1d) (together with their complex conjugates), into Eqs. (A1a) and (A1b). This operation results in two contributions to the excited populations. The first can be traced to the single-photon (SP) process. The effect of the SP process on the atomic populations is represented by the SP absorption (emission) rates:

$$a_{12}(p)=\frac{2\gamma_{12}}{\gamma_{12}^2+\delta_{12}'^2}I_{12},\quad a_{32}(p)=\frac{2\gamma_{32}}{\gamma_{32}^2+\delta_{32}'^2}I_{32},$$

where $I_{12}=|E_{12}|^2$ and $I_{32}=|E_{32}|^2$ are the corresponding laser intensities. The other is associated with the excited coherence $\rho_{31}^{(0)}(p)[\rho_{13}^{(0)}(p)]$. To trace their origin, we solve Eqs. (A1c)–(A1e) together with their complex conjugates with the goal of expressing $\rho_{31}^{(0)}(p)[\rho_{13}^{(0)}(p)]$ in terms of the population terms. This leads to

$$\rho_{31}^{(0)}(p)=\frac{E_{12}^*E_{32}}{\zeta_{31}}\left[\frac{\rho_{22}^{(0)}-\rho_{11}^{(0)}}{\nu_{21}}+\frac{\rho_{22}^{(0)}-\rho_{33}^{(0)}}{\nu_{32}}\right],\tag{14}$$

where $\zeta_{31}(p)=G_{31}(p)-iS_{31}(p)$, and

$$G_{31}(p)=\gamma_{31}+\frac{I_{32}\gamma_{12}}{\gamma_{12}^2+\delta_{12}'^2}+\frac{I_{12}\gamma_{32}}{\gamma_{32}^2+\delta_{32}'^2},\tag{15}$$

$$S_{31}(p)=\delta_{31}'+\frac{I_{32}\delta_{12}'}{\gamma_{12}^2+\delta_{12}'^2}-\frac{I_{12}\delta_{32}'}{\gamma_{32}^2+\delta_{32}'^2}.\tag{16}$$

The fact that $\rho_{31}^{(0)}(p)$ [Eq. (14)] is proportional to the product of the two field amplitudes suggests that the latter is the work of two-photon (TP) process, and can, therefore, be described by three TP absorption (emission) rates. They are, respectively, the net escaping rate of the atoms at level 1,

$$A_{11}(p)=2I_{12}I_{32}\frac{(\gamma_{12}^2-\delta_{12}'^2)G_{31}+2\gamma_{12}\delta_{12}'S_{31}}{(\gamma_{12}^2+\delta_{12}'^2)^2(G_{31}^2+S_{31}^2)};\tag{17}$$

the net escaping rate of atoms at level 3,

$$A_{33}(p)=2I_{12}I_{32}\frac{(\gamma_{32}^2-\delta_{12}'^2)G_{31}-2\gamma_{32}\delta_{32}'S_{31}}{(\gamma_{32}^2+\delta_{32}'^2)^2(G_{31}^2+S_{31}^2)};\tag{18}$$

and finally, the population exchange rate between levels 1 and 3,

$$A(p)=2I_{12}I_{32}\frac{(\gamma_{12}\gamma_{32}+\delta_{12}'\delta_{32}')G_{31}+(\gamma_{21}\delta_{12}'-\gamma_{12}\delta_{32}')S_{31}}{(\gamma_{12}^2+\delta_{12}'^2)(\gamma_{32}^2+\delta_{32}'^2)(G_{31}^2+S_{31}^2)}.\tag{19}$$

With these preparations, we reduce Eqs. (A1a) and (A1b) into steady-state rate equations, from which we express the excited populations in terms of the ground population as

$$\rho_{11}^{(0)}(p)=c_{12}(p)\rho_{22}^{(0)}(p),\rho_{33}^{(0)}(p)=c_{32}(p)\rho_{22}^{(0)}(p),\tag{20}$$

where

$$c_{12}(p)=\frac{R_{12}(\Gamma_3+R_{32})-A(\Gamma_3+A)}{(\Gamma_1+R_{12})(\Gamma_3+R_{32})-A^2},\tag{21a}$$

$$c_{32}(p)=\frac{R_{32}(\Gamma_1+R_{12})-A(\Gamma_1+A)}{(\Gamma_1+R_{12})(\Gamma_3+R_{32})-A^2},\tag{21b}$$

and

$$R_{12}(p)=a_{12}(p)-A_{11}(p),\quad R_{32}(p)=a_{32}(p)-A_{33}(p).\tag{22}$$

Finally, we combine Eqs. (A1a), (A1b), and (A1f), and transform the result with the help of Eqs. (20), into an integral equation for a single unknown function $\rho_{22}^{(0)}(p)$, in the form of

$$\begin{aligned}\gamma_t W(p)=&-\Gamma_{32}\int_{-\hbar k}^{+\hbar k}dqN(q)c_{32}\\&\times(p-\hbar k+q)\rho_{22}^{(0)}(p-\hbar k+q)\\&+\Lambda(p)\rho_{22}^{(0)}(p)-\Gamma_{12}\int_{-\hbar k}^{+\hbar k}dqN(q)c_{12}\\&\times(p+\hbar k+q)\rho_{22}^{(0)}(p+\hbar k+q),\end{aligned}\tag{23}$$

where

$$\Lambda(p)=\gamma_t+\Gamma_1c_{12}(p)+\Gamma_3c_{32}(p).$$

It is clear that once $\rho_{22}^{(0)}(p)$ is determined, the rest atomic variables can simply be obtained algebraically with the help of Eqs. (20) and (14), and additional relations in Eqs. (A1).

IV. INTEGRAL EQUATION FOR $\rho_{22}^{(0)}(P,\Delta)$

In this section, we follow the same steps in Sec. III to derive, from Eqs. (A2), an integral equation for $\rho_{22}^{(1)}(p,\Delta)$, and to establish equations necessary for the numerical calculation of $\rho_{32}^{(1)}(p,\Delta)$ and hence the absorption spectrum [Eq. (13)]. Note that in arriving at Eqs. (A2), we have introduced and shall continue to use a notational convention: a new variable $\tilde{f}(p,\Delta)$ is introduced if there exists such a function $f(p)$ in Sec. III that $f(p)=\tilde{f}(p,0)$. For example, the introduction of a variable $\tilde{\nu}_{12}(p,\Delta)$ [Eq. (A3d)] is based on the fact that $\tilde{\nu}_{12}(p,0)$ equals $\nu_{12}(p)$ [Eq. (8a)]. This convention allows Eqs. (A2) to be organized in a similar format to that of Eqs. (A1). Hence the solution to $\rho_{ij}^{(0)}(p,\Delta)$ can also be handled in a ''rate'' equation approach. Here the quotation marks serve as a reminder that the ''rates'' introduced below do not have physical meanings, and, as matter of fact, are not even real. The benefit, however, is that the solution to Eqs. (A2) can now be described in a language consistent with the description of the solution to Eqs. (A1). First we introduce two ''SP rates''

$$\tilde{a}_{12}(p,\Delta)=I_{12}\left[\frac{1}{\tilde{\nu}_{21}}+\frac{1}{\tilde{\nu}_{12}}\right],\quad \tilde{a}_{32}(p,\Delta)=I_{32}\left[\frac{1}{\tilde{\nu}_{23}}+\frac{1}{\tilde{\nu}_{32}}\right]\tag{24}$$

to account for the contributions by SP processes. Next, we trace the origin of the TP contributions to

$$\rho_{13}^{(1)}(p,\Delta)=-i\frac{E_{32}^*}{\tilde{\zeta}_{13}\tilde{\nu}_{12}}\rho_{13}^{(0)}+\frac{E_{12}E_{32}^*}{\tilde{\zeta}_{13}}\left[\frac{\rho_{22}^{(1)}-\rho_{11}^{(1)}}{\tilde{\nu}_{12}}+\frac{\rho_{22}^{(1)}-\rho_{33}^{(1)}}{\tilde{\nu}_{23}}\right], \tag{25}$$

$$\rho_{31}^{(1)}(p,\Delta)=-\frac{1}{\tilde{\zeta}_{31}}\rho_{21}^{(0)}-i\frac{E_{12}^*}{\tilde{\zeta}_{13}\tilde{\nu}_{32}}[\rho_{33}^{(0)}-\rho_{32}^{(0)}]+\frac{E_{32}E_{32}^*}{\tilde{\zeta}_{31}}\left[\frac{\rho_{22}^{(1)}-\rho_{11}^{(1)}}{\tilde{\nu}_{21}}+\frac{\rho_{22}^{(1)}-\rho_{33}^{(1)}}{\tilde{\nu}_{32}}\right], \tag{26}$$

where

$$\tilde{\zeta}_{13}(p,\Delta)=\tilde{\nu}_{13}+\frac{I_{12}}{\tilde{\nu}_{23}}+\frac{I_{32}}{\tilde{\nu}_{12}}, \tag{27a}$$

$$\tilde{\zeta}_{31}(p,\Delta)=\tilde{\nu}_{31}+\frac{I_{12}}{\tilde{\nu}_{32}}+\frac{I_{32}}{\tilde{\nu}_{21}}. \tag{27b}$$

We then introduce three TP rates

$$\tilde{A}_{11}(p,\Delta)=I_{12}I_{32}\left[\frac{1}{\tilde{\nu}_{12}^2\tilde{\zeta}_{13}}+\frac{1}{\tilde{\nu}_{21}^2\tilde{\zeta}_{31}}\right], \tag{28a}$$

$$\tilde{A}_{33}(p,\Delta)=I_{12}I_{32}\left[\frac{1}{\tilde{\nu}_{32}^2\tilde{\zeta}_{31}}+\frac{1}{\tilde{\nu}_{23}^2\tilde{\zeta}_{13}}\right], \tag{28b}$$

$$\tilde{A}(p,\Delta)=I_{12}I_{32}\left[\frac{1}{\tilde{\nu}_{12}\tilde{\nu}_{23}\tilde{\zeta}_{13}}+\frac{1}{\tilde{\nu}_{21}\tilde{\nu}_{32}\tilde{\zeta}_{31}}\right] \tag{28c}$$

to describe the TP contributions. Again, by solving the two simultaneous rate equations, we connect $\rho_{11}^{(1)}(p,\Delta)$ and $\rho_{33}^{(1)}\times(p,\Delta)$ to $\rho_{22}^{(1)}(p,\Delta)$ by the following algebraic relations:

$$\rho_{11}^{(1)}(p,\Delta)=c_{10}(p,\Delta)+\tilde{c}_{12}(p,\Delta)\rho_{22}^{(1)}(p,\Delta), \tag{29a}$$

$$\rho_{33}^{(1)}(p,\Delta)=c_{30}(p,\Delta)+\tilde{c}_{32}(p,\Delta)\rho_{22}^{(1)}(p,\Delta), \tag{29b}$$

where

$$c_{10}(p,\Delta)=\frac{\theta_1(\tilde{\Gamma}_3+\tilde{R}_{32})+\theta_2\tilde{A}}{(\tilde{\Gamma}_1+\tilde{R}_{12})(\tilde{\Gamma}_3+\tilde{R}_{32})-\tilde{A}^2}, \tag{30a}$$

$$c_{30}(p,\Delta)=\frac{\theta_2(\tilde{\Gamma}_1+\tilde{R}_{12})+\theta_1\tilde{A}}{(\tilde{\Gamma}_1+\tilde{R}_{12})(\tilde{\Gamma}_3+\tilde{R}_{32})-\tilde{A}^2}, \tag{30b}$$

and

$$\theta_1(p,\Delta)=-i\frac{E_{12}^*}{\tilde{\nu}_{12}}\left(1-\frac{I_{32}}{\tilde{\nu}_{12}\tilde{\zeta}_{13}}\right)\rho_{13}^{(0)}+\frac{E_{32}^*E_{12}}{\tilde{\nu}_{21}\tilde{\zeta}_{31}}\rho_{21}^{(0)}+i\frac{E_{32}^*I_{12}}{\tilde{\nu}_{21}\tilde{\nu}_{32}\tilde{\zeta}_{31}}(\rho_{33}^{(0)}-\rho_{22}^{(0)}), \tag{31a}$$

$$\theta_2(p,\Delta)=-\rho_{23}^{(0)}+i\frac{I_{32}E_{12}^*}{\tilde{\nu}_{23}\tilde{\nu}_{12}\tilde{\zeta}_{13}}\rho_{13}^{(0)}+\frac{E_{32}^*E_{12}}{\tilde{\nu}_{32}\tilde{\zeta}_{31}}\rho_{21}^{(0)}-i\frac{E_{32}^*}{\tilde{\nu}_{32}}\left(1-\frac{I_{12}}{\tilde{\nu}_{32}\tilde{\zeta}_{31}}\right)(\rho_{33}^{(0)}-\rho_{22}^{(0)}). \tag{31b}$$

Here, $\tilde{R}_{12}$, $\tilde{R}_{32}$, $\tilde{c}_{12}(p,\Delta)$, and $\tilde{c}_{32}(p,\Delta)$ [including $\tilde{\Lambda}(p,\Delta)$ in Eq. (32)] can be obtained by a simple transformation: placing a curly hat on every variable in the definitions for these variables in Sec. III. For example, $\tilde{R}_{12}(p,\Delta)=\tilde{a}_{12}(p,\Delta)-\tilde{A}_{11}(p,\Delta)$ corresponds to $R_{12}(p)=a_{12}(p)-A_{11}(p)$ [the first relation in Eq. (22)]. In contrast, $\theta_1(p,\Delta)$, $\theta_2(p,\Delta)$, $c_{10}(p,\Delta)$, and $c_{30}(p,\Delta)$ cannot find their analogs in Sec. III, since they depend on $\rho_{ij}^{(0)}(p)$. By combining Eqs. (A2a), (A2b), and (A2i), and with the help of Eqs. (29), we finally arrive at an equation involving integrals of a single unknown function, $\rho_{22}^{(1)}(p,\Delta)$,

$$\begin{aligned}
&-\tilde{\Gamma}_1c_{10}(p,\Delta)-\tilde{\Gamma}_3c_{30}(p,\Delta)\\
&\quad+\Gamma_2\int_{-\hbar k}^{+\hbar k}dqN(q)c_{10}(p+\hbar k+q,\Delta)\\
&\quad+\Gamma_{32}\int_{-\hbar k}^{+\hbar k}dqN(q)c_{30}(p-\hbar k+q,\Delta)\\
&=-\Gamma_{32}\int_{-\hbar k}^{+\hbar k}dqN(q)\tilde{c}_{32}(p-\hbar k+q,\Delta)\rho_{22}^{(1)}(p-\hbar k+q,\Delta)+\tilde{\Lambda}(p,\Delta)\rho_{22}^{(1)}(p,\Delta)\\
&\quad-\Gamma_{12}\int_{-\hbar k}^{+\hbar k}dqN(q)\tilde{c}_{12}(p+\hbar k+q,\Delta)\rho_{22}^{(1)}(p+\hbar k+q,\Delta),
\end{aligned} \tag{32}$$

in a format similar to Eq. (23). Once $\rho_{22}^{(1)}(p,\Delta)$ is solved, $\rho_{32}^{(1)}(p,\Delta)$ can be obtained through various algebraic relations.

V. OUTLINE OF NUMERICAL METHOD

It is now clear that the key to the solutions to Eqs. (A1) and (A2) is to develop efficient algorithms for solving Eq. (23) and (32). In this section, we show that Eq. (23) [Eq. (32)] can be cast into an inhomogeneous tridiagonal vector recurrence equation, and hence, can be solved by the method of matrix continued fraction. To begin with, we divide q between $-\hbar k$ and $+\hbar k$ into L divisions and replace the integrals in Eq. (23), with the Simpson's rule [31]. This process turns Eq. (23), into

$$\gamma_t W(n\Delta p) = -\Gamma_{32}\frac{\Delta p}{3}\sum_{l=-L}^{0} b_{l+L} N(\hbar k + l\Delta p) c_{32}((n + l)\Delta p)\rho_{22}^{(0)}((n+l)\Delta p) + \Lambda(n\Delta p)\rho_{22}^{(0)}(n\Delta p) - \Gamma_{12}\frac{\Delta p}{3}\sum_{l=0}^{L} b_l N(-\hbar k + l\Delta p) c_{12}((n + l)\Delta p)\rho_{22}^{(0)}((n+l)\Delta p), \quad (33)$$

where $p = n\Delta p$, $b_l = 4$ if l is odd, and $b_l = 2$ if l is even, with the exception that $b_0 = b_L = 1$. Note that in arriving at the form for the first integral in Eq. (33), we have made the transformation $l - L \to l$ along with the condition $L\Delta p = 2\hbar k$. Equation (33) can be put into a compact form

$$\gamma_t W(n\Delta p) = \sum_{l=-L}^{L} A_n^l \rho_{22}^{(0)}((n+l)\Delta p), \quad (34)$$

where

$$A_n^0 = \Lambda(n\Delta p) - \Gamma_{12}\frac{\Delta p}{3} N(-\hbar k) c_{12}(n\Delta p) - \Gamma_{32}\frac{\Delta p}{3} N(\hbar k) c_{32}(n\Delta p),$$

$$A_n^l = -\Gamma_{12}\frac{\Delta p}{3} b_l N(-\hbar k + l\Delta p) c_{12}((n+l)\Delta p) \quad \text{if } l > 0,$$

$$A_n^l = -\Gamma_{32}\frac{\Delta p}{3} b_{l+L} N(\hbar k + l\Delta p) c_{32}((n+l)\Delta p) \quad \text{if } l > 0.$$

By using the standard procedure [34], we transform Eq. (34) into an inhomogeneous tridiagonal vector recurrence equation

$$Q_n^- c_{n-1} + Q_n c_n + Q_n^+ c_{n+1} = r_n, \quad (35)$$

where c_n and r_n are vectors of L dimension defined as

$$c_n = \begin{pmatrix} \rho_{22}^{(0)}((Ln)\Delta p) \\ \rho_{22}^{(0)}((Ln+1)\Delta p) \\ \vdots \\ \rho_{22}^{(0)}((Ln+L-1)\Delta p) \end{pmatrix}$$

and

$$r_n = \begin{pmatrix} \gamma_t W((Ln)\Delta p) \\ \gamma_t W((Ln+1)\Delta p) \\ \vdots \\ \gamma_t W((Ln+L-1)\Delta p) \end{pmatrix},$$

respectively, while Q_n's are matrices of $L \times L$ defined as

$$(Q_n^+)^{ij} = A_{Ln+i-1}^{j-i+L}, (Q_n^-)^{ij} = A_{Ln+i-1}^{j-i-L}, (Q_n)^{ij} = A_{Ln+i-1}^{j-i},$$

with $A_n^l = 0$ if $|l| > L$. We can then solve Eq. (35) with the matrix continued fraction method [33,34]. It is apparent that the matrices involved all have the same dimension L, typically much smaller than the total number of divisions. The same algorithm can be used to obtain the solution to Eq. (32) when $\Lambda(p)$, $c_{12}(p)$, $c_{32}(p)$, and $\gamma_t W(p)$ are replaced, respectively, with $\tilde{\Lambda}(p,\Delta)$, $\tilde{c}_{12}(p,\Delta)$, $\tilde{c}_{32}(p,\Delta)$, and $-\tilde{\Gamma}_1 c_{10}(p,\Delta) - \tilde{\Gamma}_3 c_{30}(p,\Delta) + \Gamma_{12}\int_{-\hbar k}^{+\hbar k} dq N(q) c_{10}(p + \hbar k + q, \Delta) + \Gamma_{32}\int_{-\hbar k}^{+\hbar k} dq N(q) c_{30}(p - \hbar k + q, \Delta)$.

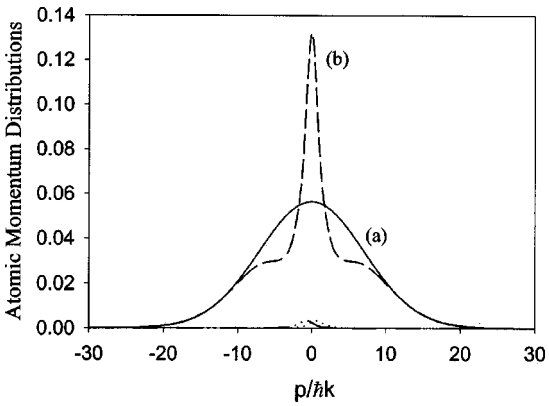

FIG. 2. (a) $W(p)$ and (b) $\rho_{22}^{(0)}(p)$ for a case of a low Rabi frequency $E_L = 0.1\Gamma$ with additional parameters $\omega_r = 0.2\Gamma$, $\gamma_t = 0.001\Gamma$, $\delta_L = -0.5\Gamma$, and $\Delta p_D = 10\hbar k$. $\rho_{11}^{(0)}(p)$ and $\rho_{33}^{(0)}(p)$ are extremely small.

VI. NUMERICAL SIMULATIONS AND DISCUSSIONS

To focus, we limit our study to symmetrical systems in which $\Gamma_{12} = \Gamma_{32} \equiv \Gamma$, $\gamma_{12} = \gamma_{32} \equiv \gamma$, $\delta_{12} = \delta_{32} \equiv \delta_L$, $E_{12} = E_{32} \equiv E_L$, and $I_{12} = I_{32} \equiv I_L$. In our simulation, $\hbar k$ is chosen to be the unit for the momentum and Γ to be the unit for any rates and frequencies; $W(p)$ is assumed to be a normalized Gaussian function,

$$W(p) = \frac{1}{\sqrt{2\pi}\Delta p_D} e^{-(p/\Delta p_D)^2}, \quad (36)$$

where Δp_D is the half-width at $\exp(-1)$; the upper and lower momentum limits are set between four and eight times $\pm\Delta p_D$ depending on the momentum spread; the momentum is sampled at a rate of ten divisions per $\hbar k$. Finally, we note a relation $\omega_D = kp/M = 2\omega_r p/\hbar k$ that might be implicitly used to make conversions between the Doppler shift ω_D and the atomic momentum p.

Figure 2 shows the momentum distributions produced under the condition that the pump fields have a low Rabi frequency ($E_L = 0.1\Gamma$) and are red detuned ($\delta_L = -0.5\Gamma$), with the rest parameters being $\omega_r = 0.2\Gamma$ and $\gamma_t = 0.001\Gamma$. At such a low Rabi frequency,

$$\Gamma, \gamma \gg a_{e2}(P) \gg A_{ee}(p), A(p) \quad (e = 1 \text{ or } 3), \quad (37)$$

so that Eqs. (21) can be approximated as $c_{e2}(p) \approx a_{e2}(p)/\Gamma \ll 1$. For this reason, the excited populations [Eqs. (20)] are almost unobservable in Fig. 2. The ground momentum distribution [Fig. 2(b)], on the other hand, experiences a significant change compared to $W(p)$ [Fig. 2(a)] due to the momentum redistribution by absorption and spontaneous emissions. The number of absorption and spontaneous emission cycles in an interaction time γ_t^{-1} can be estimated by $a_{12}(p)/\gamma_t$ under condition (37). $a_{12}(p)/\gamma_t$ equals 200 at $p_0 = |\delta_L|\hbar k/2\omega_r = 1.25\hbar k$, where the atoms are on resonance with the atomic transitions, and equals 3 at $p = 20\hbar k$. This

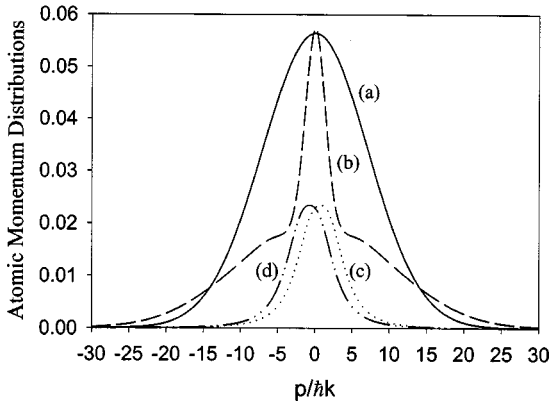

FIG. 3. (a) $W(p)$, (b) $\rho_{22}^{(0)}(p)$, (c) $\rho_{11}^{(0)}(p)$, and (d) $\rho_{33}^{(0)}(p)$ for a case of a high Rabi frequency $E_L=\Gamma$ with additional parameters the same as in Fig. 2.

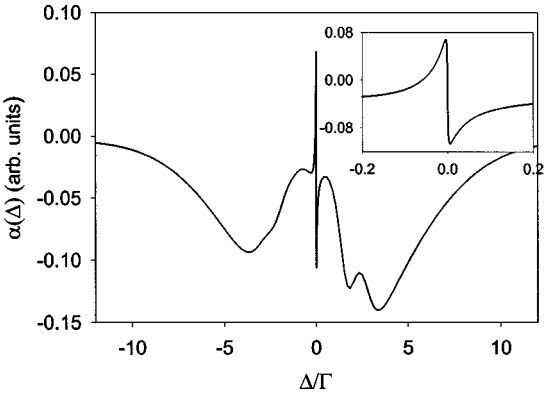

FIG. 5. The absorption spectrum corresponding to the momentum distributions in Fig. 3. The inset is an enlarged view of the Rayleigh resonance at $\Delta=0$.

difference, together with the Doppler effect, explains why the atoms around $\pm p_0$ are piled up around $p=0$ while those at large momentums are virtually untouched. Figure 3 displays the momentum distributions produced with the same parameters as in Fig. 2 except that $E_L=\Gamma$. At such a high laser intensity, $a_{e2}(0)=2\gamma I_L/(\gamma^2+\delta_L^2)\approx 1.6\Gamma>\Gamma$, so that saturation develops as is supported by Figs. 3(c) and 3(d). In addition, the narrow peak around $p=0$ in Fig. 3(b) is broader than its a counterpart in Fig. 2. This broadening is due to the ac-Stark effect, which has been incorporated into $c_{e2}(p)$ [Eq. (21)] via the two-photon rates, $A_{ee}(p)$ and $A(p)$ [Eqs. (17)–(19)]. Further, in Fig. 3, a significant heating is developed for the atoms of large momentums since there, although the cooling force is small, the momentum diffusion by spontaneous emission can still be quite large. In fact, the number of optical pumping cycles at the momentum as large as $20\hbar k$ is $a_{12}(20\hbar k)/\gamma_t\approx 30$, still quite larger than 1. The use of $a_{12}(p)/\gamma_t$ for the estimation is justified because at large momentums, inequality (37) still holds.

Figures 4 and 5 are the absorption spectra corresponding to the momentum distributions of Figs. 2 and 3, respectively. In Fig. 4, an almost homogeneously broadened line shape at the atomic transition frequency $\Omega_{32}(\Delta=-\delta_L=0.5\Gamma)$ emerges from the Doppler-broadened profile of width $\Delta\omega_D=4\Gamma(\Delta p_D=10\hbar k)$. At a laser intensity as large as in Fig. 5, this line gives way to the Rabi sidebands, as a result of the ac Stark shift. No exact formulas exist to locate the sidebands because the dressed states are now velocity dependent. However, an inspection of Fig. 5 indicates that while the two sidebands on the negative side are mixed, those on the positive side are located approximately at $+(I_L+I_L)^{1/2}\approx +1.5\Gamma$ and $+2(I_L+I_L)^{1/2}\approx +3\Gamma$, in qualitative agreement with the prediction from the dressed-atom theory for the homogeneously broadened atoms driven by resonant pump fields [25–27]. Also evident in Figs. 4 and 5 is the Rayleigh resonance of subnatural linewidth. This resonance undergoes a dramatic change as the laser intensity increases. Its shape has evolved from pro-Lorentzian (the inset in Fig. 4) to dispersionlike (the inset in Fig. 5) type. The spectrum on the red side of the Rayleigh resonance has changed from absorption to gain. Let us characterize the Rayleigh resonance with two parameters: a peak (maximum) value and a width defined as the spectroscopic distance between the peak location and $\Delta=0$ (not as the peak to peak width since no minimum can be located if the resonance is shaped in a pro-Lorentzian type like the inset in Fig. 4). Figure 6 shows how (a) the peak and (b) the width change with the pump Rabi frequency E_L (with the rest parameters the same as in Fig. 4 or 5). Both the peak and width increase with E_L up to a certain point, beyond which they begin to decrease. The width decreases at a much

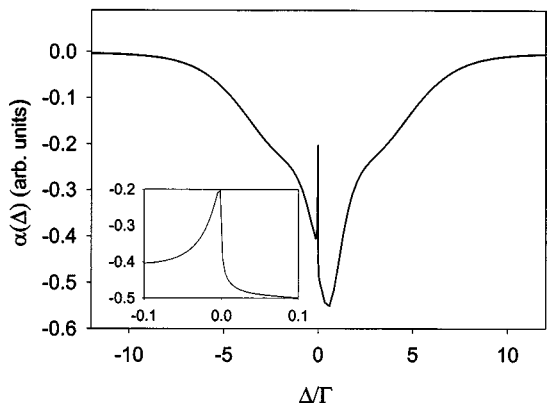

FIG. 4. The absorption spectrum corresponding to the momentum distributions in Fig. 2. The inset is an enlarged view of the Rayleigh resonance at $\Delta=0$.

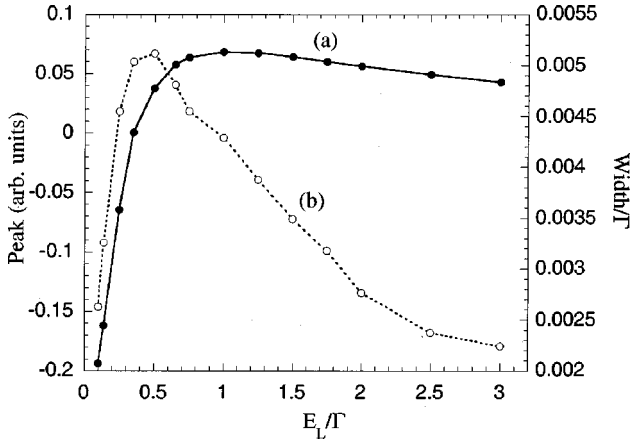

FIG. 6. The dependence of (a) the peak and (b) the width of the Rayleigh resonance on the laser Rabi frequency E_L, with additional parameters the same as in Fig. 2.

faster rate than the peak. Our simulation (not shown) indicates that the Rayleigh resonance is more of Lorentzian type at small E_L, where the peak and width experience a most dramatic increase, and is more of a dispersionlike type at large E_L, where the peak and width decrease.

To trace the origin of the Rayleigh resonance, we take the approach [11,12,39] or first discussing the concept of ''closed'' system. Let $\rho_T^{(0)}(p)=\Sigma_{i=1}^{3}\rho_{ii}^{(0)}(p)$ and $\rho_T^{(1)}(p,\Delta)=\Sigma_{i=1}^{3}\rho_{ii}^{(1)}(p,\Delta)$, respectively, be the total population and total probe-induced population modulation of a momentum group. If the Doppler width is much larger than $\hbar k$, the atomic recoil can be ignored. Under this condition, one finds from Eqs. (A1) and (A2) that

$$\rho_T^{(0)}(p)=W(p) \quad \text{and} \quad \rho_T^{(1)}(p,\Delta)=0. \tag{38}$$

Equations (38) mean that both the total population and the total probe-induced population modulation are conserved within a specific momentum group, or, equivalently, that the members of each momentum group form a closed system. This is no longer the case when the atomic recoil is taken into consideration. To illustrate this, we introduce the total population $\rho_T(t)=\int_{-\infty}^{+\infty}\Sigma_{i=1}^{3}\rho_{ii}(p,t)dp$. It can be shown from Eqs. (8) that

$$d\rho_T(t)/dt=-\gamma_t\rho_T(t)+\gamma_t.$$

Clearly, at steady state $\rho_T(t)=1$, which, together with Eq. (10), leads to two normalization conditions

$$\int_{-\infty}^{+\infty}\rho_T^{(0)}(p)=1 \quad \text{and} \quad \int_{-\infty}^{+\infty}\rho_T^{(1)}(p,\Delta)dp=0, \tag{39}$$

specific for $\rho_T^{(0)}(p)$ and $\rho_T^{(1)}(p,\Delta)$. The functions satisfying Eqs. (39) are not necessarily same as those satisfying Eqs. (38). In summary, our system is closed globally with regard to the atoms of all the momentum groups, but remains open for the atoms local to the momentum p; that is,

$$\rho_T^{(0)}(p)\neq W(p) \quad \text{and} \quad \rho_T^{(1)}(p,\Delta)\neq 0. \tag{40}$$

The spectroscopic features, apart from the Rayleigh resonance, can mostly be accounted for by the first inequality in Eq. (40). For example, the nearly homogeneously broadened line shape in Fig. 4 is a direct consequence of $\rho_T^{(0)}(p)$ being different from $W(p)$ due to laser cooling (Fig. 2). The Rayleigh resonance, on the other hand, is the work of the second inequality in Eq. (40). To illustrate this point, we divide, according to Ref. [39], $\alpha(\Delta)$ [Eq. (13)] into a recoil-induced part $\alpha_r(\Delta)$ and a background part $\alpha_b(\Delta)$. The spectroscopic terms proportional to $\rho_T^{(1)}(p,\Delta)$ are grouped into $\alpha_r(\Delta)$, while the rest all go to $\alpha_b(\Delta)$. It is evident that $\alpha_r(\Delta)$ must come from the atomic recoil since $\rho_T^{(1)}(p,\Delta)$ [consequently $\alpha_r(\Delta)$] vanishes in the absence of the atomic recoil. Such a division is carried out in Appendix B, and the results are summarized in Eqs. (B5)–(B8). Figure 7 compares $\alpha(\Delta)$, $\alpha_r(\Delta)$, and $\alpha_b(\Delta)$ for the Rayleigh resonance in Fig. 5. It shows that $\alpha_r(\Delta)$ [Fig. 7(b)] indeed determines the shape of the Rayleigh resonance while $\alpha_b(\Delta)$ [Fig. 7(c)] serves as a background offset to the total signal $\alpha(\Delta)$ [Fig. 7(a)]. In fact, this behavior holds for all the examples given in this paper.

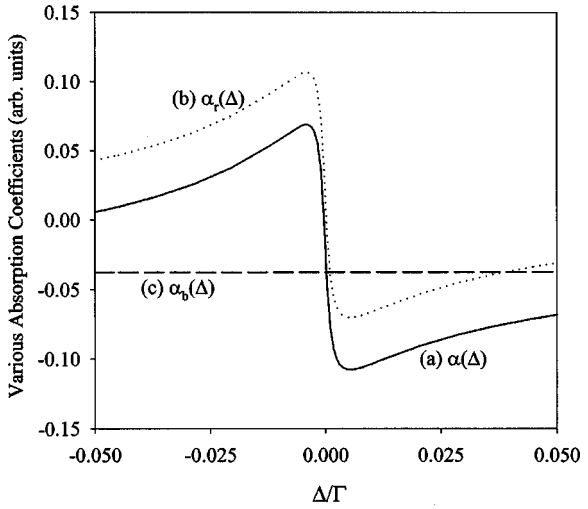

FIG. 7. The decomposition of (a) $\alpha(\Delta)$ into a recoil-induced part (b) $\alpha_r(\Delta)$ and a background part (c) $\alpha_b(\Delta)$ for the Rayleigh resonance corresponding to Fig. 5.

The line shape of $\alpha_r(\Delta)$ depends critically on $\rho_T^{(1)}(p,\Delta)$. In Fig. 8, we display several real $[\rho_T^{(1)}(p,\Delta)]$ with different Δ using the same parameters as in Fig. 5. First, the area under each curve is zero, in accordance with the second relation in Eq. (39). Second, as $|\Delta|$ increases, $\rho_T^{(1)}(p,\Delta)$ diminishes quickly. This can be understood as follows [9,23,24]. The combined field of the probe and copropagating fields oscillates at a beat frequency Δ. As a result, the population is modulated with the same frequency. The modulation depth of the total population of a momentum group is the amplitude of $\rho_T^{(1)}(p,\Delta)$. This population grating (in the time domain) contributes to the absorption spectrum by scattering part of the pump field into the component at the frequency and along the direction of the probe field. If the combined field oscillates much faster than the system can respond, the response of the system will be weak. In another words, if $|\Delta|\gg 1/\tau$, where τ characterizes the response time of the system, the amplitude of $\rho_T^{(1)}(p,\Delta)$ will be small. The maximum response happens approximately around $|\Delta|\approx 1/\tau$. Since γ_t^{-1} is viewed as the interaction time, we expect that

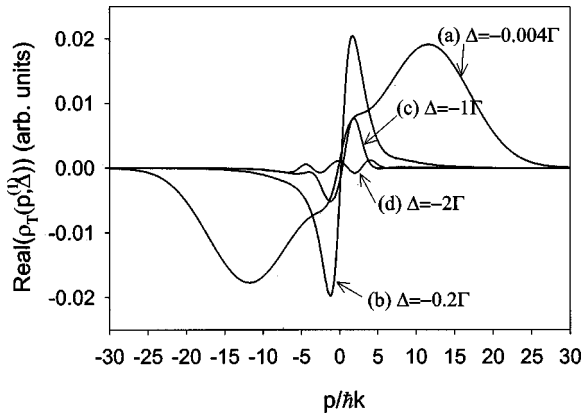

FIG. 8. The real part of $\rho_T^{(1)}(p,\Delta)$ as a function of momentum p for (a) $\Delta=-0.004\Gamma$, (b) $\Delta=-0.2\Gamma$, (c) $\Delta=-\Gamma$, and (d) $\Delta=-2\Gamma$. The rest of the parameters are the same as in Fig. 3 (or Fig. 5).

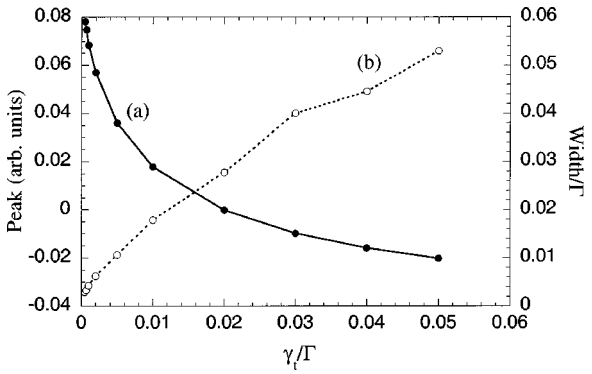

FIG. 9. The dependence of (a) the peak and (b) the width of the Rayleigh resonance on the transit decay rate γ_t. The rest parameters are the same as in Fig. 3 (or Fig. 5).

in our system τ^{-1} be proportional to γ_t. Consequently, as illustrated in Fig. 9, as γ_t increases, the width [Fig. 9(b)] and peak [Fig. 9(a)] of the Rayleigh line increase and decrease, respectively.

VII. SUMMARY

In this paper, we have developed a numerical method by which V systems driven by nearly resonant counterpropagating pump fields can be analyzed in the momentum regime where a full quantum-mechanical treatment of the atomic variables is necessary. This method consists of first reducing the steady-state GOB-type equations into a single integral equation whose solution holds the key to the rest atomic variables, second transforming the integral equation into an inhomogeneous tridiagonal vector recurrence equation, and finally solving it by the method of matrix continued fraction. This has the advantage of limiting the dimension of the matrices to the number of divisions in $2\hbar k$, a subspace typically much smaller than the entire momentum space. Equipped with this method, we have performed numerical studies of the momentum distribution in the absence of the probe field, and, in particular, the absorption spectrum in the copropagating spectrum configuration, with our research interest being focused on recoil-related phenomena. The effect of the atomic recoil has been demonstrated with examples both at low and relatively high pump laser intensities. In particular, the origin of the Rayleigh resonance of subnatural linewidth has been traced to the spectroscopic contribution associated with the total probe-induced population modulation of a specific momentum group, $\rho_T(p,\Delta)$. However, we are unable to obtain any analytical descriptions of the resonance, due partly to the fact that, in the nearly resonant interaction, both $\rho_{22}^{(0)}(p)$ and $\rho_{22}^{(1)}(p,\Delta)$ have to be determined in a self-consistent manner. For this reason, this study only gives a limited view of the dependence of the Rayleigh resonance on the atom-field parameters. In a future studies, we hope to gain further insight into the formation of the Rayleigh resonance of subnatural linewidth by developing asymptotic expressions that can give better guidance to numerical investigations.

ACKNOWLEDGMENT

This work was supported by a grant from Research Corporation.

APPENDIX A: STEADY-STATE EQUATIONS

$\rho_{ij}^{(0)}(p)$ satisfies the following set of coupled equations:

$$\Gamma_1\rho_{11}^{(0)}(p)=i[E_{12}\rho_{21}^{(0)}(p)-\text{c.c.}], \tag{A1a}$$

$$\Gamma_3\rho_{33}^{(0)}(p)=i[E_{32}\rho_{23}^{(0)}(p)-\text{c.c.}], \tag{A1b}$$

$$\nu_{12}(p)\rho_{12}^{(0)}(p)=iE_{12}[\rho_{22}^{(0)}(p)-\rho_{11}^{(0)}(p)]-iE_{32}\rho_{13}^{(0)}(p), \tag{A1c}$$

$$\nu_{32}(p)\rho_{32}^{(0)}(p)=iE_{32}[\rho_{22}^{(0)}(p)-\rho_{33}^{(0)}(p)]-iE_{12}\rho_{31}^{(0)}(p), \tag{A1d}$$

$$\nu_{31}(p)\rho_{31}^{(0)}(p)=i[E_{32}\rho_{21}^{(0)}(p)-E_{12}^{*}\rho_{32}^{(0)}(p,t)], \tag{A1e}$$

$$\begin{aligned}\gamma_t\rho_{22}^{(0)}(p)=&\Gamma_{12}\int_{-\hbar k}^{+\hbar k}dqN(q)\rho_{11}^{(0)}(p+\hbar k+q)\\&+\Gamma_{32}\int_{-\hbar k}^{+\hbar k}dqN(q)\rho_{33}^{(0)}(p-\hbar k+q)+\gamma_tW(p),\\&-i[E_{12}\rho_{21}^{(0)}(p)-\text{c.c.}]-i[E_{32}\rho_{23}^{(0)}-\text{c.c.}],\end{aligned} \tag{A1f}$$

$$\rho_{ij}^{(0)}(p)=\rho_{ji}^{(0)*}(p), \quad \text{if } i\neq j. \tag{A1g}$$

The coupled equations for $\rho_{ij}^{(1)}(p,\Delta)$ are

$$\tilde{\Gamma}_1(\Delta)\rho_{11}^{(1)}(p,\Delta)=i[E_{12}\rho_{21}^{(1)}(p,\Delta)-E_{12}^{*}\rho_{12}^{(1)}(p,\Delta)], \tag{A2a}$$

$$\begin{aligned}\tilde{\Gamma}_3(\Delta)\rho_{33}^{(1)}(p,\Delta)=&-\rho_{23}^{(0)}(p)+i[E_{32}\rho_{23}^{(1)}(p,\Delta)-E_{32}^{*}\rho_{32}^{(1)}\\&\times(p,\Delta)],\end{aligned} \tag{A2b}$$

$$\begin{aligned}\tilde{\nu}_{21}(p,\Delta)\rho_{21}^{(1)}(p,\Delta)=&-iE_{12}^{*}[\rho_{22}^{(1)}(p,\Delta)-\rho_{11}^{(1)}(p,\Delta)]\\&+iE_{32}^{*}\rho_{31}^{(1)}(p,\Delta),\end{aligned} \tag{A2c}$$

$$\begin{aligned}\tilde{\nu}_{12}(p,\Delta)\rho_{12}^{(1)}(p,\Delta)=&\rho_{13}^{(0)}(p)+iE_{12}[\rho_{22}^{(1)}(p,\Delta)-\rho_{11}^{(1)}(p,\Delta)]\\&-iE_{32}\rho_{13}^{(1)}(p,\Delta),\end{aligned} \tag{A2d}$$

$$\begin{aligned}\tilde{\nu}_{23}(p,\Delta)\rho_{23}^{(1)}(p,\Delta)=&-iE_{23}^{*}[\rho_{22}^{(1)}(p,\Delta)-\rho_{33}^{(1)}(p,\Delta)]\\&+iE_{12}^{*}\rho_{13}^{(1)}(p,\Delta),\end{aligned} \tag{A2e}$$

$$\begin{aligned}\tilde{\nu}_{32}(p,\Delta)\rho_{32}^{(1)}(p,\Delta)=&[\rho_{33}^{(0)}(p)-\rho_{22}^{(0)}(p)]+iE_{32}[\rho_{22}^{(1)}(p,\Delta)\\&-\rho_{33}^{(1)}(p,\Delta)]-iE_{12}\rho_{31}^{(1)}(p,\Delta),\end{aligned} \tag{A2f}$$

$$\tilde{\nu}_{13}(p,\Delta)p_{13(p,\Delta)}^{(1)}=-i[E_{32}^{*}\rho_{12}^{(1)}(p,\Delta)-E_{12}\rho_{23}^{(1)}(p,\Delta)], \tag{A2g}$$

$$\begin{aligned}\tilde{\nu}_{31}(p,\Delta)\rho_{31}^{(1)}(p,\Delta)=&-\rho_{21}^{(0)}(p)+i[E_{32}\rho_{21}^{(1)}(p,\Delta)-E_{12}^{*}\rho_{32}^{(1)}\\&\times(p,\Delta)],\end{aligned} \tag{A2h}$$

$$\tilde{\gamma}_t(\Delta)\rho_{22}^{(1)}(p,\Delta)=\rho_{23}^{(0)}(p)-i[E_{12}\rho_{21}^{(1)}(p,\Delta)-E_{12}^{*}\rho_{12}^{(1)}\times(p,\Delta)]-i[E_{32}\rho_{23}^{(1)}(p,\Delta)-E_{32}^{*}\rho_{32}^{(1)}\times(p,\Delta)]+\Gamma_{12}\int_{-\hbar k}^{+\hbar k}N(q)\rho_{11}^{(1)}(p+\hbar k+q,\Delta)dq+\Gamma_{32}\int_{-\hbar k}^{+\hbar k}N(q)\rho_{33}^{(1)}(p-\hbar k+q,\Delta)dq, \tag{A2i}$$

where

$$\tilde{\Gamma}_1(\Delta)=-i\Delta+\Gamma_1, \tag{A3a}$$

$$\tilde{\Gamma}_3(\Delta)=-i\Delta+\Gamma_3, \tag{A3b}$$

$$\tilde{\gamma}_t(\Delta)=-i\Delta+\gamma_t, \tag{A3c}$$

$$\tilde{\nu}_{12}(p,\Delta)=\gamma_{12}-i[\Delta+\delta_{12}'(p)], \tag{A3d}$$

$$\tilde{\nu}_{32}(p,\Delta)=\gamma_{32}-i[\Delta+\delta_{32}'(p)], \tag{A3e}$$

$$\tilde{\nu}_{31}(p,\Delta)=\gamma_{31}-i[\Delta+\delta_{31}'(p)], \tag{A3f}$$

$$\tilde{\nu}_{ji}(p,\Delta)=\gamma_{ij}-i[\Delta-\delta_{ij}'(p)], \quad \text{if } i\neq j. \tag{A3g}$$

APPENDIX B: DERIVATION OF $\alpha_R(\Delta)$ AND $\alpha_B(\Delta)$

As a first step, we replace $\rho_{31}^{(1)}(p,\Delta)$ in Eq. (A2f) with Eq. (26), and solve for $\rho_{32}^{(1)}(p,\Delta)$, with the result

$$\rho_{32}^{(1)}(p,\Delta)=\frac{1}{\tilde{\nu}_{32}}\left(1-\frac{I_1}{\tilde{\zeta}_{31}\tilde{\nu}_{32}}\right)\left(\rho_{33}^{(0)}-\rho_{22}^{(0)}+i\frac{E_{12}}{\tilde{\nu}_{32}\tilde{\zeta}_{31}}\rho_{21}^{(0)}-i\frac{I_{12}E_{32}}{\tilde{\zeta}_{31}\tilde{\nu}_{32}\tilde{\nu}_{21}}(\rho_{22}^{(1)}-\rho_{11}^{(1)})+i\frac{E_{32}}{\tilde{\nu}_{32}}\left(1-\frac{I_{12}}{\tilde{\zeta}_{31}\tilde{\nu}_{32}}\right)\times(\rho_{22}^{(1)}-\rho_{33}^{(1)}). \tag{B1}$$

Next, we insert Eqs. (29) into the definition for $\rho_T^{(1)}(p,\Delta)=\Sigma_{i=1}^{3}\rho_{ii}^{(1)}(p,\Delta)$ to obtain

$$\rho_{22}^{(1)}(p,\Delta)=-\frac{c_{10}+c_{30}}{1+\tilde{c}_{12}+\tilde{c}_{32}}+\frac{1}{1+\tilde{c}_{12}+\tilde{c}_{32}}\rho_T^{(1)}(p,\Delta), \tag{B2}$$

which, together with relations (29), leads to

$$\rho_{11}^{(1)}(p,\Delta)=\frac{c_{10}(1+\tilde{c}_{32})-c_{30}\tilde{c}_{12}}{1+\tilde{c}_{12}+\tilde{c}_{32}}+\frac{\tilde{c}_{12}}{1+\tilde{c}_{12}+\tilde{c}_{32}}\rho_T^{(1)}(p,\Delta), \tag{B3}$$

$$\rho_{33}^{(1)}(p,\Delta)=\frac{c_{30}(1+\tilde{c}_{12})-c_{10}\tilde{c}_{32}}{1+\tilde{c}_{12}+\tilde{c}_{32}}+\frac{\tilde{c}_{32}}{1+\tilde{c}_{12}+\tilde{c}_{32}}\rho_T^{(1)}(p,\Delta). \tag{B4}$$

By inserting Eqs. (B2)–(B4) into Eq. (B1) and separating the terms proportional to $\rho_T^{(1)}(p,\Delta)$ from the rest, we find that $\rho_{32}^{(1)}(p,\Delta)=\rho_{32}^{(1)}(p,\Delta)_b+\rho_{32}^{(1)}(p,\Delta)_r$, where

$$\rho_{32}^{(1)}(p,\Delta)_b=\frac{1}{\tilde{\nu}_{32}}\left(1-\frac{I_{12}}{\tilde{\zeta}_{31}\tilde{\nu}_{32}}\right)(\rho_{33}^{(0)}-\rho_{22}^{(0)})+i\frac{E_{12}}{\tilde{\nu}_{32}\tilde{\zeta}_{31}}\rho_{21}^{(0)}+i\frac{I_{12}E_{32}}{\tilde{\zeta}_{31}\tilde{\nu}_{32}\tilde{\nu}_{21}}\left[\frac{(c_{10}+c_{30})(1+\tilde{c}_{12})}{1+\tilde{c}_{12}+\tilde{c}_{32}}+c_{10}\right]-i\frac{E_{32}}{\tilde{\nu}_{32}}\left(1-\frac{I_{12}}{\tilde{\zeta}_{31}\tilde{\nu}_{32}}\right)\left[\frac{(c_{10}+c_{30})(1+\tilde{c}_{32})}{1+\tilde{c}_{12}+\tilde{c}_{32}}+c_{30}\right] \tag{B5}$$

and

$$\rho_{32}^{(1)}(p,\Delta)_r=-i\rho_T^{(1)}(p,\Delta)\frac{E_{32}}{\tilde{\nu}_{32}(1+\tilde{c}_{12}+\tilde{c}_{32})}\left[\frac{I_{12}}{\tilde{\zeta}_{31}\tilde{\nu}_{21}}(1-\tilde{c}_{12})+\left(\frac{I_{12}}{\tilde{\zeta}_{31}\tilde{\nu}_{32}}-1\right)(1-\tilde{c}_{32})\right]. \tag{B6}$$

Accordingly, the absorption spectrum is divided into $\alpha(\Delta)=\alpha_b(\Delta)+\alpha_r(\Delta)$, where

$$\alpha_b(\Delta)=\int\rho_{32}^{(1)}(p,\Delta)_b dp, \tag{B7}$$

$$\alpha_r(\Delta)=\int\rho_{32}^{(1)}(p,\Delta)_r dp. \tag{B8}$$

[1] See, for example, *Laser Cooling and Trapping of Atoms*, special issue of J. Opt. Soc. Am. B **6** (1989), edited by S. Chu and C. Wieman.

[2] M. H. Anderson, J. R. Fnsher, M. R. Mathews, C. E. Wieman, and E. A. Cornell, Science **269**, 198 (1995).

[3] C. C. Bradly, C. A. Sackett, J. J. Tollet, and R. G. Hulet, Phys. Rev. Lett. **75**, 1687 (1995).

[4] K. B. Davis, M.-O. Mewes, M. R. Andrews, N. J. Van Druten, D. S. Durfee, D. M. Kurn, and W. Ketterle, Phys. Rev. Lett. **75**, 3969 (1995).

[5] A. S. Parkins and D. F. Walls, Phys. Rep. **303**, 1 (1998), and references therein.

[6] C. I. Westbrook, R. N. Watts, C. E. Tanner, S. L. Rolston, W. D. Phillips, P. D. Lett, and P. L. Gould, Phys. Rev. Lett. **65**, 33 (1990).

[7] D. Grison, B. Lounis, C. Salomon, J. Y. Courtois, and G. Grynberg, Europhys. Lett. **15**, 149 (1991).

[8] J. W. R. Tabosa, G. Chen, Z. Hu, R. B. Lee, and H. J. Kimble, Phys. Rev. Lett. **66**, 3245 (1991).

[9] P. Verkerk, B. Lounis, C. Salomon, and C. Cohen-Tannoudji,

Phys. Rev. Lett. **68**, 3861 (1992).
[10] J.-Y. Courtois and G. Grynberg, Phys. Rev. A **46**, 7060 (1992).
[11] J. Guo, P. R. Berman, and B. Duketsky, Phys. Rev. A **46**, 1426 (1992).
[12] J. Guo and P. R. Berman, Phys. Rev. A **47**, 4128 (1993).
[13] J.-Y. Courtois, G. Grynberg, B. Lounis, and P. Verkerk, Phys. Rev. Lett. **72**, 3017 (1994).
[14] R. Bonifacio and L. D. Salvo, Nucl. Instrum. Methods Phys. Res. A **341**, 360 (1994).
[15] R. Bonifacio, L. D. Salvo, L. M. Narducci, and E. J. D'Angelo, Phys. Rev. A **50**, 1716 (1994).
[16] R. Bonifacio and L. D. Salvo, Opt. Commun. **115**, 505 (1995).
[17] G. L. Lippi, G. P. Barozzi, S. Barbay, and J. R. Tredicce, Phys. Rev. Lett. **76**, 2452 (1996).
[18] P. R. Hemmer, N. P. Bigelow, D. P. Katz, M. S. Shahriar, L. DeSalvo, and R. Bonifacio, Phys. Rev. Lett. **77**, 1468 (1996).
[19] L. D. Salvo, R. Cannerozzi, R. Bonifacio, E. J. D'Angelo, and L. M. Narducci, Phys. Rev. A **52**, 2342 (1995).
[20] M. G. Moore and P. Meystre, Phys. Rev. A **58**, 3248 (1998).
[21] P. R. Berman, Phys. Rev. A **59**, 585 (1999).
[22] Y. Castin, H. Wallis, and J. Dalibard, J. Opt. Soc. Am. B **6**, 2046 (1989).
[23] B. Lounis, J.-Y. Courtois, P. Verkerk, C. Salomon, and G. Grynberg, Phys. Rev. Lett. **69**, 3029 (1992).
[24] J.-Y. Courtois and G. Grynberg, Phys. Rev. A **48**, 1378 (1993).
[25] C. Cohen-Tannoudji and S. Reynaud, J. Phys. B **10**, 2311 (1977).
[26] C. Cohen-Tannoudji and S. Reynaud, J. Phys. B **10**, 365 (1977).
[27] L. M. Narducci, M. O. Scully, G.-L. Oppo, P. Ru, and J. R. Tredicce, Phys. Rev. A **42**, 1630 (1990).
[28] H. Y. Ling, Phys. Rev. A **59**, 3714 (1999).
[29] S. Stenholm, Appl. Phys. **15**, 287 (1978).
[30] S. Haroche and F. Hartmann, Phys. Rev. A **6**, 1280 (1972).
[31] W. H. Press, B. P. Flannery, S. A. Teukolsky, and W. T. Vetterling, *Numerical Recipes in C* (Cambridge University Press, New York, 1988).
[32] S. Stenholm and J. Javanainen, Appl. Phys. **16**, 159 (1978).
[33] S. Stenholm, *Fundations of Laser Spectroscopy* (Wiley, New York, 1984).
[34] H. Risken, *The Fokker-Plack Equation* (Springer-Verlag, New York, 1989).
[35] V. G. Minogin and O. T. Serimaa, Opt. Commun. **30**, 373 (1979).
[36] T. Cai and N. P. Biglow, Opt. Commun. **104**, 175 (1993).
[37] C. J. Bordè, in *Advances in Laser Spectroscopy*, edited by F. S. T. Arrechi and H. Walther (Plenum, New York, 1983).
[38] Y. R. Shen, *The Principles of Nonlinear* Optics (Wiley, New York, 1984).
[39] M. Gorlicki, P. R. Berman, and G. Khitrova, Phys. Rev. A **37**, 4340 (1988).